PNAS RESEARCH ARTICLE | MEDICAL SCIENCES

Limb girdle muscular disease caused by *HMGCR* mutation and statin myopathy treatable with mevalonolactone

Yuval Yogev[a], Zamir Shorer[b], Arie Koifman[c], Ohad Wormser[a], Max Drabkin[a], Daniel Halperin[a], Vadim Dolgin[a], Regina Proskorovski-Ohayon[a], Noam Hadar[a], Geula Davidov[d,e], Hila Nudelman[d], Raz Zarivach[d,e], Ilan Sheleff[f], Yonatan Perez[a], and Ohad S. Birk[a,c,1]

Edited by Lawrence Steinman, Stanford University, Stanford, CA; received October 27, 2022; accepted January 4, 2023

Myopathy is the main adverse effect of the widely prescribed statin drug class. Statins exert their beneficial effect by inhibiting HMG CoA-reductase, the rate-controlling enzyme of the mevalonate pathway. The mechanism of statin myopathy is yet to be resolved, and its treatment is insufficient. Through homozygosity mapping and whole exome sequencing, followed by functional analysis using confocal microscopy and biochemical and biophysical methods, we demonstrate that a distinct form of human limb girdle muscular disease is caused by a pathogenic homozygous loss-of-function missense mutation in HMG CoA reductase (*HMGCR*), encoding HMG CoA-reductase. We biochemically synthesized and purified mevalonolactone, never administered to human patients before, and establish the safety of its oral administration in mice. We then show that its oral administration is effective in treating a human patient with no significant adverse effects. Furthermore, we demonstrate that oral mevalonolactone resolved statin-induced myopathy in mice. We conclude that *HMGCR* mutation causes a late-onset severe progressive muscular disease, which shows similar features to statin-induced myopathy. Our findings indicate that mevalonolactone is effective both in the treatment of hereditary *HMGCR* myopathy and in a murine model of statin myopathy. Further large clinical trials are in place to enable the clinical use of mevalonolactone both in the rare orphan disease and in the more common statin myopathy.

HMGCR | statins | limb girdle muscular dystrophy | mutation

Significance

Limb girdle muscular dystrophies (LGMD) are a group of genetic diseases, whose causative mutations are only partly known, with no currently available definitive treatment. Statins, a lipid-lowering drug class, act by inhibiting HMG-CoA reductase, encoded by *HMGCR*, and show a common side effect—myopathy. The cause of statin myopathy is mostly unknown and treatment is limited. We show that a severe progressive hereditary myopathy, greatly overlapping with statin myopathy, is caused by *HMGCR* mutation. We demonstrate that treatment with oral mevalonolactone, never used to treat patients before, is effective and safe both in *HMGCR*-myopathy in humans and statin-myopathy in mice. Thus, this work sheds light on molecular pathways of statin myopathy and LGMD, delineating effective specific treatment for both.

Limb girdle muscular dystrophies (LGMDs) are rare, mostly progressive, autosomal diseases that share proximal muscle weakness as the major attribute. Most LGMDs present with elevated creatinine kinase (CK) and myopathic electromyographic features (1, 2). Disease is usually progressive to a variable degree, ranging from minor disability to complete inability to ambulate, and can involve the large proximal muscles, as well as axial and facial muscles. Different forms of LGMD may exhibit skeletal muscle hypertrophy, kyphoscoliosis, and contractures or involve other muscle groups and manifest with distal weakness, cardiomyopathy, dysphagia, and respiratory difficulties. Other features may include intellectual disability (*TRAPPC11*; Mendelian Inheritance in Man (MIM) #615356), seizures (*LAMA2*, MIM #618138), arrhythmia (*BVES*, MIM #616812), and ocular anomalies (*POMT1*; MIM #609308). LGMD syndromes show a wide range of genetic heterogeneity, with over 40 known disease-associated genes. The pathophysiological processes underlying different LGMDs vary, and are broadly linked to disorders in structure of the sarcolemma, integration with extracellular matrix, nuclear or plasma membrane stability, or mechanical sensing and signal transduction. Currently, there is no available treatment for any of the LGMDs other than supportive care, but treatment modalities are being developed, and several trials of genetic therapy are ongoing (1–3).

Statins, a lipid-lowering drug class which is of the most commonly prescribed medications in the world, act through inhibition of HMG-CoA reductase. The main adverse effect of statins is myopathy (4, 5). While reports differ on this matter, up to 30% of statin users suffer from statin-associated muscle symptoms (SAMS), occasionally causing life threatening rhabdomyolysis or immune mediated necrotizing myositis (IMNM) (6–9). Statins have also been implicated in nonmuscle adverse events, such as diabetes mellitus, cancer, cognitive impairment, and liver damage (10). We now describe a form of severe late-onset progressive limb girdle muscle disease, caused by a mutation in HMG CoA reductase (*HMGCR*), mimicking statin-induced myopathy. We synthesized and purified mevalonolactone, the product of HMGCR enzymatic activity, and show that given orally, it is effective in treatment of human *HMGCR*-muscle disease as well as in treating statin-induced myopathy in mice, with no significant adverse effects.

Author contributions: Y.Y. and O.S.B. designed research; Y.Y., Z.S., A.K., O.W., M.D., D.H., V.D., R.P.-O., N.H., G.D., H.N., Y.P., and O.S.B. performed research; Y.Y. contributed new reagents/analytic tools; Y.Y., R.Z., I.S., and O.S.B. analyzed data; and Y.Y. and O.S.B. wrote the paper.

Competing interest statement: The authors have patent filings to disclose, A patent has been filed by Y.Y. and O.S.B. Otherwise, the authors have declared that no conflict of interests exists.

This article is a PNAS Direct Submission.

[1]To whom correspondence may be addressed. Email: obirk@bgu.ac.il.

This article contains supporting information online at https://www.pnas.org/lookup/suppl/doi:10.1073/pnas.2217831120/-/DCSupplemental.

Published February 6, 2023.

Results

A Form of Autosomal Recessive Limb Girdle Muscle Disease Is Caused by *HMGCR* Mutation. Six individuals of a single consanguineous Bedouin kindred (Fig. 1*A*) were affected with apparently autosomal recessive progressive limb girdle muscle disease. The disease initially manifested during the fourth decade of life with pain on exertion, followed by muscle fatigue and weakness, affecting mostly the proximal and axial muscles, and culminating with involvement of respiratory muscles. Notably, the patients showed only mild atrophy of affected muscles, with flaccid muscle tone and no contractures. The oldest three patients (V:2,5,12 ages 49, 58, and 51 y, respectively) were wheelchair-bound or bedridden and suffered from respiratory insufficiency; patient V:2 was chronically ventilated by tracheostomy. Distal and facial muscles were mostly spared in all patients, and none suffered from any other neurological deficits or dysphagia (details in *SI Appendix*, Table S1).

Central nervous system imaging studies were normal. MRI, computerized tomography (CT), and ultrasound scans showed various levels of atrophy with severe fatty replacement of large proximal skeletal muscles and axial muscles with sparing of the distal and facial muscles (Fig. 1*B* and *SI Appendix*, Fig. S5). These radiological features are highly reminiscent of the MRI features of end stage statin myopathy and immune-mediated necrotizing myopathy (IMNM) without edema (11–15). EMG studies of four patients showed a myopathic pattern, and motor nerve conduction velocity (NCV) demonstrated normal distal latencies, amplitudes, and velocities. There were no clear signs of cardiomyopathy, although four patients showed slightly elevated troponin T levels, and two demonstrated conduction abnormalities in ECG; cardiac, and chest CT scans done for patients V:9 and V:5 were normal, and echocardiography in four patients showed no abnormalities. Abdominal ultrasound was normal in patients V:2, V:5, and V:9.

Pathological evaluation of biopsies taken from the biceps or deltoid muscles of three patients, at a time where weakness was evident, were stained with H&E, Gomori trichrome, NADH, ATPase at 3 pH levels, Cytochrome oxidase (COX), SDH, basic fuchsin-methylene blue, and for dystrophins 1 to 3. Histopathological evaluation did not reveal any pathological features such as fibrosis or inflammation, with the exception of mild deficiency of type-II muscle fibers in one patient, possibly indicating a muscle degeneration and regeneration pattern (Fig. 1*C*). Thin section electron microscopy was normal as well.

Blood tests showed muscle injury with elevated creatine kinase (up to over 250-fold upper level of normal CK; maximal CK 35761U/L, patient V:8) and moderately elevated transaminases in all patients. An occasional mild rise in alkaline phosphatase was observed in patients with severe phenotypes. While the CK levels were augmented compared to most other forms of muscular

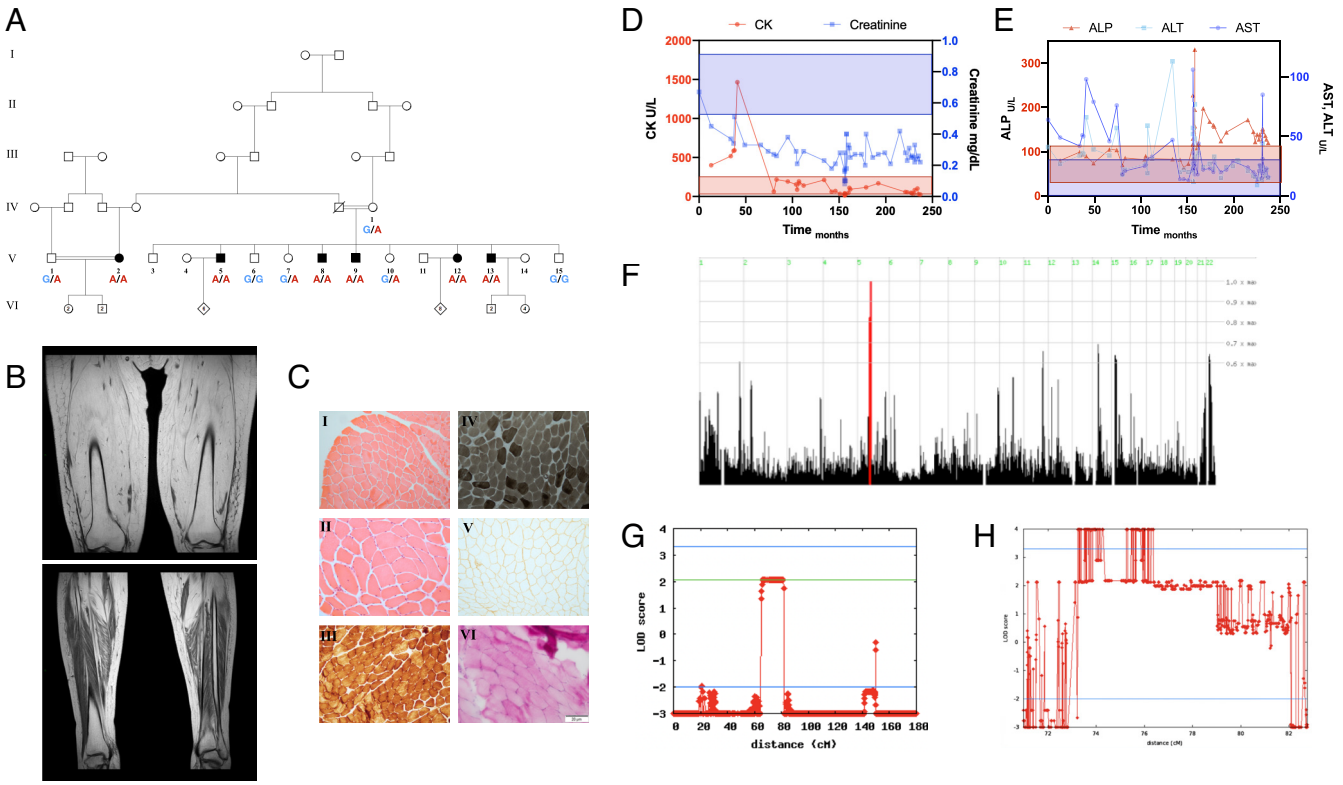

Fig. 1. Pedigree, phenotype, and linkage analysis. (*A*) Pedigree of a Bedouin kindred from the Negev region of Israel, showing six individuals affected by adult-onset LGMD, (*B*) T1 MRI imaging of the thighs and legs of patient V:2 at age 49, showing complete atrophy of skeletal muscles of the thigh with fatty replacement, and partial sparing of the distal muscles of the legs. Additional imaging can be seen in *SI Appendix*, Fig. S5. (*C*) Deltoid muscle histology of patient V:2 at age 34, when muscles showed marked weakness; blood tests and EMG indicated myopathy. I–II: H&E staining showing normal morphology with no necrosis, fibrosis or inflammation, III: COX stain showing normal COX activity, IV: ATPase pH 9.4 stain showing mild deficiency of type II muscle fibers, V: Dystrophin III stain showing normal distribution, VI: PAS stain showing no accumulation of glycogen. Other stains did not demonstrate marked features, as described. (*D* and *E*) Serum enzymes of patient V:2 over 21 y, starting with disease onset at age 31. Shading represents the reference range of the color-matched test. (*D*) As the CK levels dropped into the normal range and eventually below, creatinine levels dropped as well, indicating very low muscle mass. (*E*) ALT and AST levels decreased over the course of disease, following muscle damage, while ALP levels rose late. Acute spikes in ALT, AST, and ALP levels coincided with hospital and ICU admissions, possibly indicating disease flare-ups. (*F*) Homozygosity mapping showing a homozygous locus in chromosome 5 shared by all affected individuals but not other tested family members. (*G*) Reduced complexity multipoint linkage analysis chart of chromosome 5, showing the shared locus (*H*) Two-point linkage analysis chart of the 3.2 Mbp locus and adjacent regions, showing a LOD score higher than four.

dystrophies, the rise in alkaline phosphatase is not uncommon (16). With disease progression and muscular atrophy, CK levels gradually normalized and eventually even dropped beneath normal limits, alongside a simultaneous drop in creatinine levels, consistent with low skeletal muscle mass (Fig. 1*D*). Cholesterol and lipoprotein levels were not elevated (*SI Appendix*, Table S1), with most patients frequently showing total cholesterol levels lower than 120 mg/dL. All patients had elevated fasting blood glucose levels above 126 mg/dL, with patient V:2 treated with insulin. Other than muscle symptoms and high blood glucose levels, no other overt pathologies were shared between patients.

Genome-wide linkage analysis, through single nucleotide polymorphism (SNP) genotyping for all available family members, identified a single 3.2 Mbp homozygous segment on chromosome 5q13.2-q13.3, that was shared among all affected individuals and was either absent or in a heterozygous state in unaffected individuals (Fig. 1*F*). The disease-associated locus, spanning between SNPs rs2129403 and rs2914143, 5:73803333-77084175 (GRCh38/hg38), showed a maximal logarithm of the odds (LOD) score of 4.8204 at rs4345300 (Fig. 1 *G* and *H*).

Filtering through whole-exome sequencing data of patients V:13 and V:2 (*Methods*), only a single variant was found within the 3.2 Mbp locus: g.5:75359992G>A (GRCh38/hg38); NM_000859.3:c.2465G>A; p.(G822D) in *HMGCR* (Fig. 2*A*). The variant is a singleton, is not present in large genomic databases, predicted to be pathogenic according to SIFT and PolyPhen2 algorithms, and has a CADD score of 29.6. The homozygous mutated nucleotide, coded amino acid and the entire gene sequence are highly conserved throughout evolution (Fig. 2 *B* and *C*). The Glycine to Aspartate substitution at position 822 is a radical replacement, predicted to interfere with several peptide bonds, disrupt helix-dipole, and cause charge-based repulsion, with possible detrimental impact on secondary and tertiary structure of HMG-CoA reductase (Fig. 2*D*). No other variants were found in the 3.2 Mbp locus, and no other LGMD and LGMD-like associated variants were detected.

The *HMGCR* variant was validated by restriction analysis and Sanger sequencing (Fig. 2*A*) and was found to fully segregate as expected for autosomal recessive mode of inheritance. Using restriction fragment length polymorphism (RFLP), we confirmed that within a cohort of 190 nonrelated, ethnically matched controls, none carried the variant. Screening of 20 individuals of the same tribe did not show additional carriers.

Due to the proximity of the disease-associated locus with the *SMN* gene which is known to cause Spinal-Muscular Atrophy, and albeit dissimilar clinical characteristics, we conducted a thorough analysis of *SMN1* and *SMN2*, including multiplex ligation-dependent probe amplification (MLPA) for copy number analysis, RFLP for common mutations, and differential whole gene sequencing, which demonstrated a complete lack of *SMN2* gene but no variations in *SMN1*.

Mutated HMG-CoA Reductase Shows Reduced Function. *HMGCR* is ubiquitously expressed, with increased levels in the skin, adrenal-gland, and different parts of the gastrointestinal (GI) tract (Fig. 2*E*). The encoded protein, HMG-CoA reductase, has a key role in the mevalonate pathway and facilitates the rate-limiting step in cholesterol synthesis, i.e., the reduction of HMG-CoA to mevalonic acid and free coenzyme A.

We set out to test functional effects of the *HMGCR* mutation. We introduced the human c.2465G>A, p.(G822D) mutation to SH-SY5Y cells using CRISPR knock-in (KI), and showed by confocal microscopy that the mutation does not change the subcellular localization of the protein (Fig. 3 *A* and *B*). However,

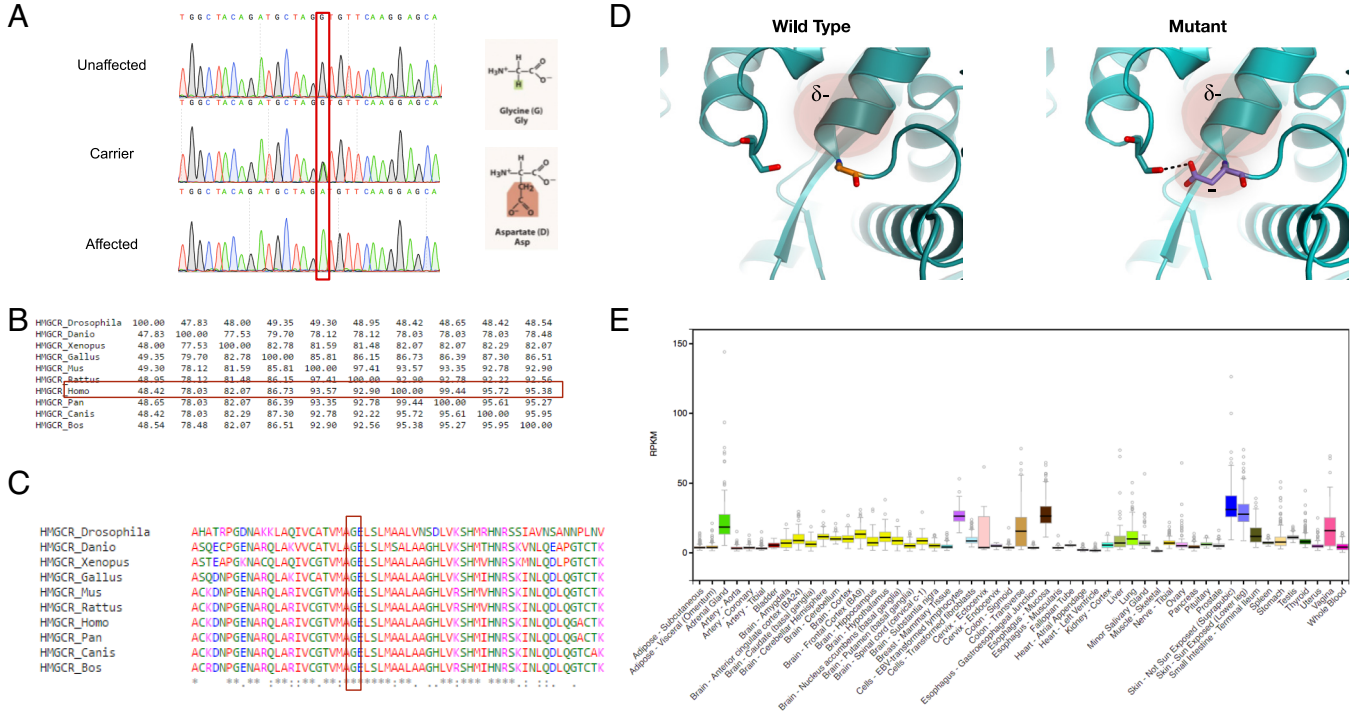

Fig. 2. The *HMGCR* mutation. (*A*) Sanger sequencing of an *HMGCR* amplicon of an unaffected individual (V:6), an obligatory carrier (IV:1) and an affected individual (V:13). The mutation causes a glycine to aspartate nonconservative substitution at position 822. (*B*) Precent identity matrix of *HMGCR* produced using ClustalOmega, showing high homology between the human *HMGCR* and orthologs. (*C*) Multiple alignment of human *HMGCR* and orthologs produced using ClustalOmega, showing that the substituted amino acid is highly conserved throughout evolution. (*D*) Structural model of HMG CoA-reductase protein in the WT and mutated form, based on 1DQ8. The substitution presumably forms a new H-bond with a distal residue, compromises the helix dipole, and causes electrostatic repulsion. (*E*) Expression of *HMGCR* across various tissues, obtained using the GTEx database.

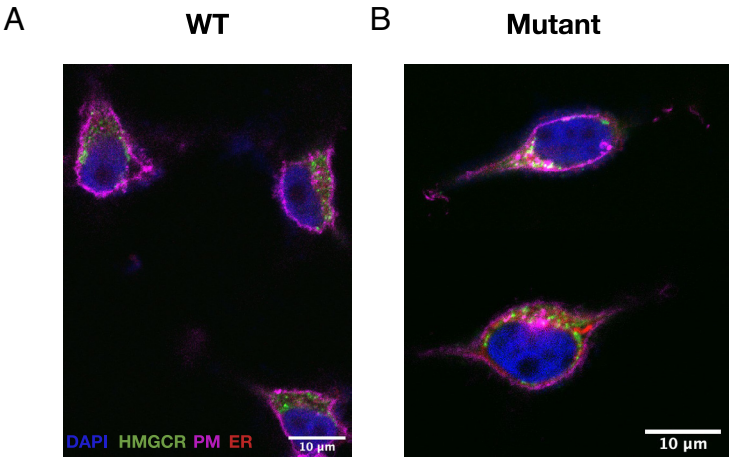

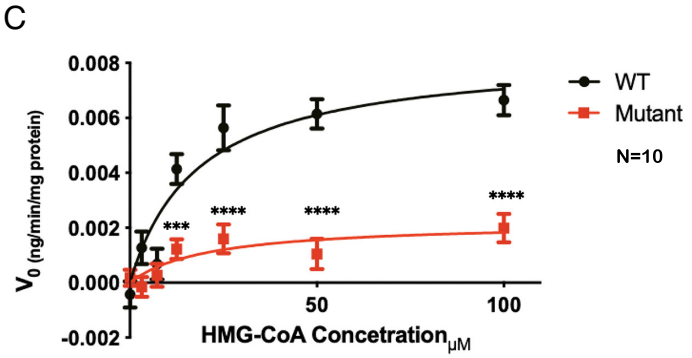

D

	WT	Mutant
Vmax (ng/min/mg protein)	7.28±0.56	2.29±0.49
Km (µM)	13.73±3.83	22.66±8.27

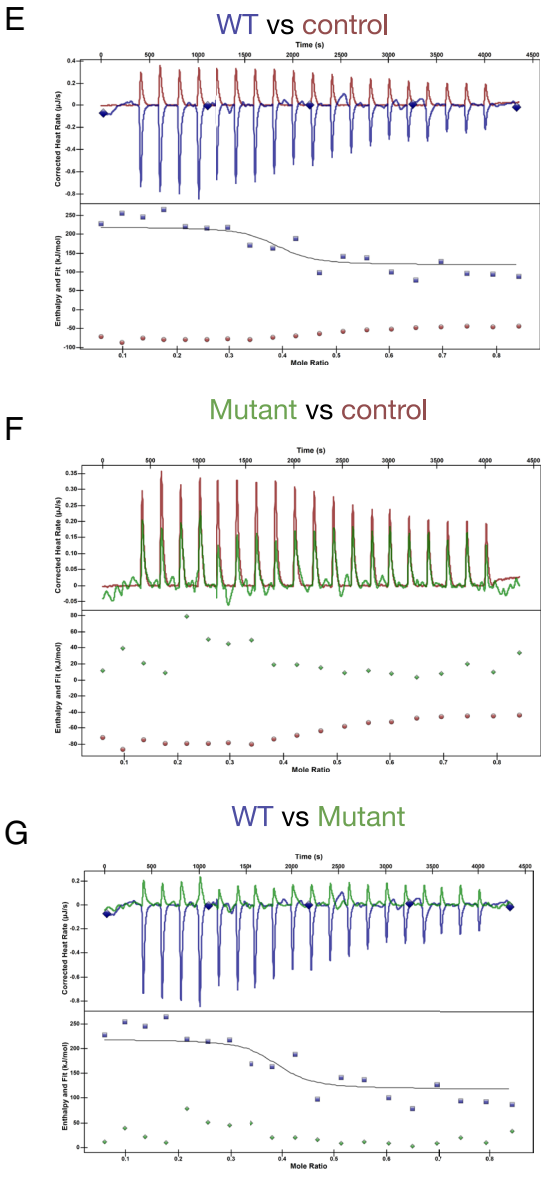

Fig. 3. *HMGCR* mutation impairs protein function. (*A* and *B*) Subcellular localization of WT (*A*) and CRISPR-KI mutant (*B*) HMGCR in SH-SY5Y cells. Both WT and mutant HMGCR protein (green) are located in clusters in the cytoplasm with some relation to the endoplasmic reticulum (red). (*C* and *D*) HMGCR enzymatic activity. The velocity of enzymatic reduction of different concentrations of HMG CoA was measured by spectrophotometric NADPH oxidation assay of the WT (n = 9) and mutant (n = 12) forms of HMGCR. Analyzed using Michaelis–Menten analysis and multiple *t*-tests. (*E*–*G*) Mutant HMGCR shows decreased affinity to pravastatin, a protein inhibitor that binds to the same catalytic pocket as HMG CoA (n = 8). As seen, mutant kinetics are almost identical to the no protein control. PM, plasma membrane; ER, endoplasmic reticulum.

spectro-colorimetric analysis of the wild-type (WT) and mutant proteins' function using an NADPH-oxidation assay demonstrated that compared to its WT counterpart, the mutant protein had 69% reduction in V_{max} and 65% increase in K_m in relation to the substrate HMG-CoA, indicating lower affinity of the mutated protein for HMG-CoA, as well as overall slower reaction-rate (Fig. 3 *C* and *D*). This was also supported by ITC analysis of HMG-CoA reductase thermodynamics to a known inhibitor, pravastatin: the overall thermodynamic values of the ITC assay, using HMG-CoA as the analyte, reflect both binding of the substrate to HMGCR, as well as the thermodynamics of the reduction reaction. To overcome this, we used pravastatin, a statin that is known to inhibit HMGCR by binding to the same catalytic pocket as HMG-CoA (17) (Fig. 3 *E*–*G*). While the WT protein exhibited a mild exothermic reaction, the mutant form displayed kinetics almost identical to a no-protein control, indicating that the catalytic pocket of the mutant protein has a very low affinity toward pravastatin. To conclude, the *HMGCR* variant was found to be pathogenic according to American College of Medical Genetics (ACMG) criteria PM2, PP3, PS3, PP4, and PP1 (moderate to strong) (18). The pathogenicity of the variant is further established by the subjective and objective response to treatment, as described hereinafter.

Oral Mevalonate Treatment in *HMGCR*-Limb Girdle Muscle Disease. Drawing from animal studies of *HMGCR* mutations (19), we initiated a treatment trial of the human *HMGCR*-disease with the downstream metabolite of HMG-CoA reductase, mevalonate. As detailed in Methods, the lactone form of mevalonate, mevalonolactone, not available as a pharmaceutical preparation, was produced in-house by batch-fermentation and was purified to over 94% (*SI Appendix*, Figs. S2 and S3). Impurities were analyzed and were all ascertained as nonhazardous. To assess the safety of oral mevalonolactone treatment, we performed a toxicological

assay by oral gavage in naive wild-type C57BL/6 mice. Mice were given doses up to 2 g/kg/d, more than five times the maximal weekly dose we intended for human use. Mevalonolactone was administered to mice for 7 d, after which they were killed, and blood, GI tract, liver, and muscle samples were examined. No major differences between groups were seen (*SI Appendix*, Fig. S6 *A–K*).

Due to the severe state of patients and the lack of alternative treatment options, oral mevalonolactone treatment trial was approved by the Israeli ministry of health (MOH) under an expanded use/compassion treatment procedure. The treatment trial was approved initially for a single patient, V:2, who was in the most severe state, with possible expansion to other patients based on clinical outcomes. Prior to initiation of treatment, thorough neurological exam by an experienced neurologist, imaging studies, electrophysiological studies, and blood work were conducted. Alongside severe limb girdle myopathy and total dependence on respiratory support in V:2, a notable finding was the lack of anti-HMGCR antibodies in any of the patients (Fig. 4*A*). No other rheumatological abnormalities were detected (*SI Appendix*, Table S1). Serum mevalonolactone level of patient V:2 was 14.5 to 29.1% than the normal average (Fig. 4*B*).

The initial treatment plan included a single weekly oral dose of mevalonolactone, a viscous liquid, diluted in tap water starting at 2 mg/kg/wk with a weekly doubling up to 400 mg/kg/wk (*SI Appendix*, Fig. S4). However, since subjective and objective improvement was noticed, the dose was maintained at 16 mg/kg, given up to three times a week. Mevalonolactone oral uptake was found to be very rapid: the mevalonate levels began to rise 20 min after oral administration, peaked at 50 min, and returned to baseline levels 2 h after ingestion (Fig. 4*C*).

During treatment, there was improvement in muscle strength as assessed by dynamometry and by manual muscle testing (MMT) performed by an experienced neurologist (Fig. 4 *D–L* and Video S1). Progressive improvement was noticed among all muscle groups as early as 21 d from initiation of treatment, with the greatest subjective improvement seen in the deltoid muscles. Distal muscles of the lower limb showed normal strength at the beginning of the trial and were not assessed by dynamometry after 3 mo into the trial (Fig. 4 *J–L*). Respiratory muscles were assessed by spirometry, which demonstrated marked increase in peak expiratory flow (+265%; from 6 to 22% of predicted value), forced vital capacity (+342%; from 17.4 to 77.6% of predicted value), and FEV1 (+345%, from 10.7 to 48.1% of predicted value, Fig. 4*M*). In addition to objective measurements of muscle strength, there was remarkable improvement in independence and function in activities of daily living. To mention some—patient V:2, previously unable to perform any of these tasks, was now able to raise herself from lying sideways to a sitting position, to fully abduct her arm when laying, to extend her knees to 150°, to feed her grandchild on her own and to stand with

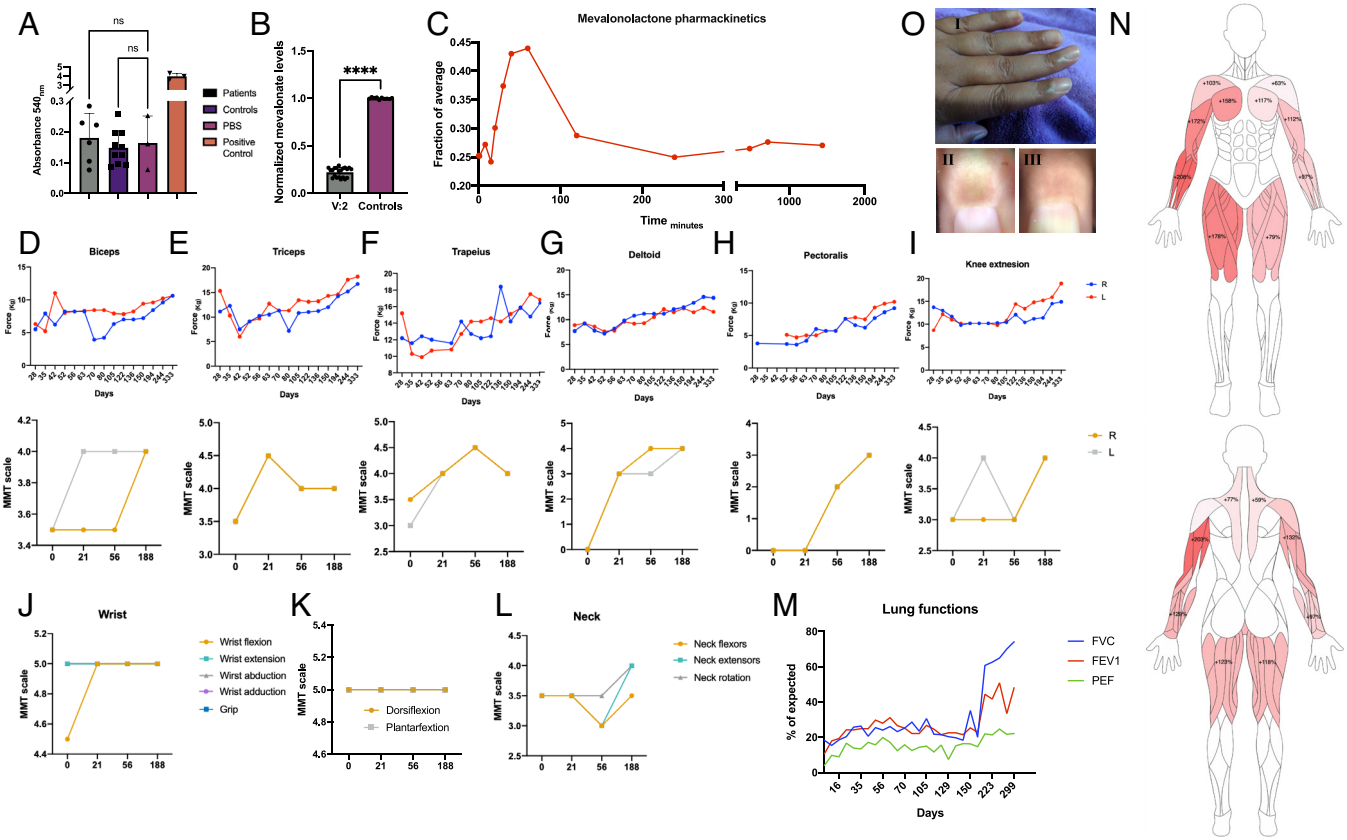

Fig. 4. Oral mevalonolactone treatment in human *HMGCR*-LGMD. (*A*) Anti-HMGCR autoantibodies titer in patients (n = 6) and healthy controls (n = 10). (*B*) Plasma mevalonolactone levels of patients V:2 (n = 20 on multiple occasions) and healthy controls (n = 10), normalized to average level of controls. (*C*) Mevalonolactone levels in peripheral blood of V:2 after an oral dose of 16 mg/kg mevalonolactone, normalized to average level of controls. (*D–I*) Evaluation of muscle strength of patient V:2 throughout the treatment period by dynamometry (*Top*) and manual muscle test (MMT; *Bottom*) by an experienced neurologist. (*J–L*) Evaluation of distal muscles throughout the treatment by an experienced neurologist. (*M*) Lung functions throughout the treatment period assessed by spirometry. (*N*) Muscle strength improvement "heat-map" by dynamometry, precent improvement from weakest state. (*O*) Pigmentation in the proximal nail fold which appeared occasionally following treatment. I: Gross appearance; II: Dermatoscopic image of the index finger showing pigmentation; and III: Dermatoscopic image of the same index finger several days later, pigmentation has resolved. Statistical analysis using *t*-test.

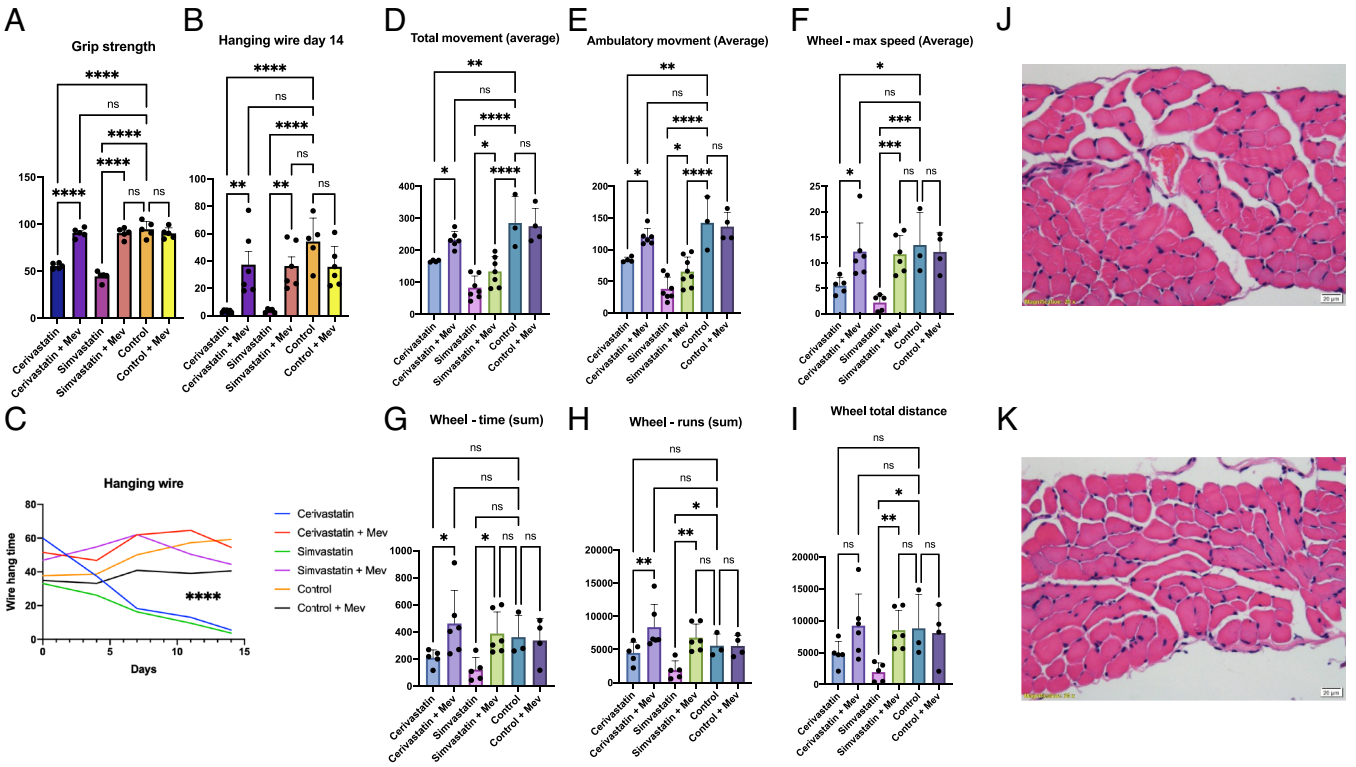

Fig. 5. Oral mevalonolactone treatment in murine statin-induced myopathy. Mice were treated daily with intraperitoneal injections of either Cerivastatin, Simvastatin, or 0.9% saline solution for 14 d, with or without 200 mg/kg oral mevalonolactone. n = 4 in each group. Mice were housed in PhenoMaster cages for the last 3 d of treatment. (*A*) Grip strength test on day 14. (*B*) Hanging wire test on day 14. (*C*) Hanging wire test throughout the study. (*D*–*I*) Measurements of strength and endurance from PhenoMaster cages. (*J*–*K*) H&E stained diaphragm muscles of a subject from the Cerivastatin group (*J*) and the Cerivastatin + mevalonolactone group (*K*). No signs of fibrosis, necrosis, or inflammation were evident. Diaphragm, gastrocnemius, and quadriceps muscles were examined from two subjects in every group. Statistical analysis using one-way ANOVA with multiple comparisons.

assistance. Her respiratory muscles also improved, and she was able to breath without her ventilator for over 3 h while maintaining SpO_2 >96%.

Adverse effects to the treatment were minimal. Throughout the 1-y treatment period, the patient reported occasional gastrointestinal symptoms, including mild nausea, diarrhea, and constipation, urinary tract infections, a single occasion of near syncope, moderate headaches, rare temporary occurrences of a subjective sensation of limb swelling and of dilation of small veins in the upper and lower limbs which were not evident in objective measurements. None of these episodes were unusual in frequency or severity compared to pretreatment, and none could be directly related to the treatment, required medical treatment, or hospitalization. However, noticeable pigmentation of the proximal nail fold was seen on four different occasions in direct relation to treatment (Fig. 4*O*). The discoloration appeared hours after treatment and vanished after 2 to 3 d of mevalonolactone ingestion and did not appear to be in relation to any vascular insufficiency, as assessed by presence of peripheral pulses, normal capillary refill, absence of pain, and point-of-care doppler ultrasonography (Vscan extend, GE Healthcare). With the continuation of treatment, this effect subsided but did appear after dose escalation and after intermissions in treatment regimen. To our knowledge, this phenomenon is not known to occur with any current drug treatments. Cholesterol, HDL, and LDL levels did not show significant change during treatment. Mevalonolactone treatment is currently ongoing, and the expanded access program is being considered for remaining patients. The subjective and objective response to mevalonolactone treatment further helps to establish the pathogenic role of the *HMGCR* variant (20).

Mevalonolactone Treatment Shows Reduction of Symptoms in a Model of Statin Myopathy. HMG-CoA reductase is the drug target of statins, whose most common adverse effect, statin-induced myopathy, affects up to 30% of treated patients (6). Given our demonstration of the apparent safety of mevalonolactone oral treatment in the hereditary *HMGCR* human disease, we assessed its utility in the treatment of a more prevalent condition, statin myopathy, employing a murine model of severe statin-induced myopathy (21, 22). Mice given statins showed decreased muscle strength and endurance as assessed by wire hanging and grip force tests (Fig. 5 *A* and *B*) and a lower tendency to initiate and pursue movement as observed in measurements of total ambulation, voluntary wheel activity, and maximal speed. Animals that were treated with statins and given free access to mevalonolactone-supplemented drinking water (*Methods*) showed a greatly reduced phenotype, most prominently observed in the hanging wire experiments (Fig. 5 *B* and *C* and Video S2). Muscle histology of mice treated with statins with or without mevalonolactone did not show overt signs of necrosis or inflammation (Fig. 5 *J* and *K*). This is in line with the histopathological specimens of *HMGCR* mutation patients, which did not show gross abnormalities, and, with histological findings in biopsy samples of statin-related myopathy patients, which often do not show pathological features (23–26).

Discussion

We describe a form of autosomal recessive progressive limb girdle muscle disease and demonstrate through genetic, statistical, and functional studies that it is caused by a partial loss-of-function missense mutation in *HMGCR*, encoding a key enzyme of the mevalonate pathway (https://www.intechopen.com/media/

chapter/48175/media/image3.jpg). While genome-wide association studies (GWAS) showed *HMGCR* polymorphisms to be associated with total cholesterol and lipoprotein levels and response to statin use, this is the first description of a human disease caused by a mutation in *HMGCR*. Genetic perturbations in nonhuman *HMGCR* orthologs have been associated with severe phenotypes; while complete knockout of the mouse ortholog causes prenatal lethality (27), conditional muscle-specific null mutants display a severe muscular phenotype (19).

Pharmacological inhibition of HMG CoA-reductase with drugs of the statin class is associated with myalgia and myopathy, up to rhabdomyolysis, which is potentially fatal (6–9). The *HMGCR* hereditary disease patients described here present with a phenotype that shows a high overlap with SAMS. Moreover, intermediate to severe SAMS usually present with proximal muscle weakness, further delineating the similarity to the *HMGCR* disease (25). One major difference between SAMS and the hereditary *HMGCR* disease is the relatively acute onset of SAMS compared with the insidious presentation of muscle symptoms in the *HMGCR*-limb girdle muscle disease. However, chronic or subacute presentation of SAMS or severe statin myopathy have been described and may mimic LGMD (25, 28).

HMGCR-limb girdle muscle disease presents roughly at the fourth decade of life. It is unclear as to what causes this delayed onset of symptoms. Notably, LGMDs comprise a heterogenous group of diseases and may develop at variable ages (2), and SAMS are more common and severe in advanced ages (23). The timing of onset may be linked to accumulated damage over the years, to lower anabolic activity, anabolic signaling, or to other unknown causes. This notion might also serve to explain in part the fact that despite the short half-life of mevalonolactone in blood, it showed a lasting effect. As to the short half-life of mevalonolactone, there were no apparent subjective or objective fluctuations in muscle symptoms during the periods between treatment administration, further highlighting the lasting effect of mevalonolactone. It is possible that mevalonolactone enables long-lasting structural or physiological changes, while another possibility is that it is rapidly redistributed to tissues; that is, the rapid clearance of mevalonolactone from the blood might be due to a high volume of distribution rather than a short half-life.

Notably, in our small cohort, it appears that female patients were affected in a more severe manner and at a younger age (*SI Appendix*, Table S1). Interestingly, female sex is associated with greater risk of developing statin myopathy (9, 15, 29). The cause of gender differences in statin myopathy and possibly in *HMGCR*-LGMD is unknown but may be related to overall lower muscle mass ratio in females or lower exercise tolerance. As statins were previously suggested to partially act by altering testosterone levels (30), this may also be attributed to endocrine differences, i.e., lower androgen levels.

Statin use was linked to increased risk of developing type II diabetes mellitus (31). Notably, all six *HMGCR*-LGMD patients had at least one fasting blood sugar level >126 mg/dL, albeit only one (V:2) had overt diabetes with glucose levels >300 mg/dL (*SI Appendix*, Table S1). While a direct correlation must not be assumed, insulin resistance might be another feature of *HMGCR*-LGMD. Intriguingly, blood cholesterol levels in the *HMGCR*-LGMD patients were low, yet within the normal range, likely due to the mutation only partially abrogating HMG CoA-reductase activity, as well as dietary uptake of exogenous cholesterol.

The cause of SAMS is currently unknown. A variety of proposed mechanisms for the adverse effect of statins on skeletal muscles include paucity of downstream metabolites of the mevalonate pathway, such as Coenzyme Q10, farnesyl pyrophosphate, geranylgeranyl pyrophosphate, and of cholesterol, and the placebo effect (32), as well as a mechanism for severe statin-induced myopathy by immune reaction mediated by anti-HMGCR autoantibodies, leading to IMNM (15). In relation to these proposed mechanisms, anti-HMGCR autoantibodies were not detected in our patients, and cholesterol levels were not abnormally low, suggesting that alternative pathological processes are underlying *HMGCR*-LGMD, and perhaps SAMS. These findings suggest that SAMS and *HMGCR*-LGMD may be associated with metabolic alterations that induce accumulating damage. Other drugs which inhibit enzymes of the mevalonate pathway, such as bisphosphonates, are not known to cause myalgia or myopathy, possibly indicating that other disturbances in metabolic flux are responsible for this phenomenon.

The relatively benign pathological features in histopathological evaluation of muscle tissue are intriguing and, with the exception of mild type II fiber deficiency seen in one patient, did not show additional abnormal findings. While this is consistent with findings in statin myopathy patients (23–26), it hinders formal classification of the disease described here as LGMD at this point (33). This could possibly be attributed to the early timing of biopsy during the disease course or nonoptimal selection of the biopsy site. As seen in CT and MRI imaging later in the course of disease, severe atrophy and fatty infiltration were evident in the large proximal muscles, indicating severe dystrophic changes. Due to the lack of clinical need, no further biopsies were collected.

In the current study, we demonstrate the feasibility of oral mevalonolactone treatment. To the best of our knowledge mevalonolactone has never been used before to treat human patients, and so, there is no available knowledge as to its safety, dosage, and efficacy. The current study was limited to a single patient suffering from severe *HMGCR*-LGMD, where no treatments are available. Mevalonolactone treatment of *HMGCR*-LGMD was shown to be effective, with objective and subjective improvement in daily function, in contrast with the progressive nonremitting deterioration evident in the natural course of the disease. As this was an open label trial, the treatment regimen is still open to further improvement. In this case, there were a multitude of factors hindering optimal treatment—such as poor adherence of V:2 to treatment and relative reluctance to perform physical activity, and the deteriorated baseline status of skeletal muscles prior to initiation of the treatment, defined in radiological interpretation of MRI studies as "severe atrophy;" there is also room for possible further optimization of quantity or frequency of mevalonolactone dosing. The treatment trial is ongoing and is being considered for more patients under an expanded access protocol. Notably, throughout the 1 y of oral administration of mevalonolactone, there were no significant adverse effects in direct relation to treatment. One unique side effect of treatment was transverse hyperpigmentation of the nailbeds, which occurred in proximity to dose escalation and rapidly self-resolved. Despite our efforts and consultation with several experts, we have yet to elucidate the basis of this phenomenon.

Lastly, we demonstrated that in a murine model, oral mevalonolactone protected from the myotoxicity induced by high-dose statin treatment. Current treatment of SAMS in mild cases consists solely of discontinuation of statin therapy, which is most often successful, with possible rechallenge if symptoms resolve; treatment of rhabdomyolysis is mostly supportive, and treatment of IMNM may include corticosteroids, Methotrexate, IVIGs, and Rituximab, with variable levels of success. Since many medical facilities lack the ability to detect anti-HMGCR antibodies, and for the lack of better treatment modalities, seronegative patients may be treated with immunosuppression.

In light of our findings, pending larger clinical trials, mevalonolactone is the first specific treatment effective in any LGMD; furthermore, pending larger clinical trials, it might offer a safe and

effective treatment in cases of SAMS that persist after statin cessation, as well as cases of severe SAMS including rhabdomyolysis, and perhaps even IMNM.

Materials and Methods

Clinical Phenotyping. This study was approved by the Soroka University Medical Center (SUMC) IRB. Blood samples for DNA, RNA, and various other tests were obtained from patients (six) and unaffected (six) family members following informed consent. Clinical phenotyping was determined by experienced neurologists and geneticist for all affected individuals, and genetic counseling was offered to direct family members. Imaging studies, electromyography (EMG), NCV studies, and muscle biopsies were conducted in accordance with common standards of medical practice and using common techniques.

Genetic Analysis. Genome-wide linkage analysis of eight family members was performed as previously described (34) using Homozygosity-Mapper (35) and SUPERLINK ONLINE SNP 1.1 (36).

Whole-exome sequencing of individuals V:2 and V:13 (Fig. 1*A*) was performed at a mean coverage of 100-fold, using SureSelect Human All Exon V6+UTR enrichment kit (Agilent) for target enrichment. Otherwise, sequencing and WES data analysis were performed as previously described (34).

Validation and Segregation Analysis. Validation and segregation analysis of the *HMGCR* variant c.2306G>A; NM_000859.3 (ClinVar accession number SCV002758004) was done using Sanger sequencing and RFLP analysis. PCR primers sequences are available in supplementary *SI Appendix*, Table S2. The *HMGCR* c.2306G>A variant along with the modification in "RFLP Reverse" primer introduces a Bsp1286I restriction site: restriction analysis of the 258-bp wild-type allele amplicon yields two fragments (218 and 40 bp), whereas the mutant allele amplicon remains uncut.

Protein Purification. *HMGCR* transcript NM_000859.3 was cloned from human skeletal muscle cDNA (Takara™) into pJET vector using CloneJET PCR cloning kit (Thermo Scientific™) (see *SI Appendix*, Table S2 for primer list and *SI Appendix*, Table S3 for plasmid list). Site-directed mutagenesis was performed by PCR using standard technique and the mutagenesis primers in *SI Appendix*, Table S2, introducing the p.(G822D) variant. The catalytic portion of HMGCR (p.426-888) was subcloned into pGEX-6p plasmid (Cytiva™). Protein expression and purification were performed as described by Istvan et al. (37) with minor modifications. Briefly, pGEX-6P-HMGCR-426-888 was transformed to *Escherichia coli* BL21 cells. Cells were grown in 2xYT broth with 0.5M sorbitol and 2.5 mM betaine and 100 mg/L ampicillin in 6L batches until OD_{600} = 0.6, after which expression was induced with 0.5M IPTG and collected after 16 h. Cell pellets were resuspended in buffer A (*SI Appendix*, Table S4–solutions and buffers) and disrupted using a FRENCH® Press (Thermo), and cleared lysates were purified by affinity chromatography using Pierce™ Glutathione Agarose (Thermo), washed with buffer B and either eluted with Buffer B with added glutathione or washed with buffer E, digested on-column with HRV3C protease (SAE0045, Sigma), and then eluted with buffer E. Protein was further purified using ÄKTAprime plus (Cytiva) system, using size exclusion on a SuperDex200 column, followed by ion exchange using a Hitrap Q HP column with buffers C and D. Lastly, purified protein was dialyzed and concentrated using Amicon® column (Merck-Millipore) and buffer E, and aliquots of purified protein in buffer E were flash-frozen at a concentration of 0.6 mg/mL. The purified protein was analyzed by western blot with a rabbit monoclonal anti-HMGCR antibody (SAB4200528, Sigma; *SI Appendix*, Fig. S1)

HMG CoA Reductase Catalytic Assay. HMG CoA reductase enzymatic activity was assessed by a colorimetric assay. HMG CoA reductase reactions were set up in 96 well plates, with each well containing a total volume of 100 µL Buffer E, supplemented with 400 µM NADPH (sigma) and 2 µL of either WT or mutant-purified HMG CoA reductase protein (0.6 mg/mL), WT enzyme with pravastatin, or a no enzyme control. Reactions were initiated by the addition of HMG-CoA substrate to a final concentration of 0 to 400 µM. Immediately after the addition of HMG-CoA, plates were analyzed for 340 nm absorbance using an Infinite M200 plate reader (Tecan). Absorbance was monitored every 30 s for a total of 90 min. For repeat experiments, HMG CoA was added to either WT or mutant reactions in an alternating fashion in order to minimize technical variations of V_0.

Isothermal Calorimetric Analysis. Isothermal calorimetry (ITC) studies were performed on a nano-ITC instrument (TA Instruments). In order to facilitate pure substrate binding measurements and to avoid the reaction generated by HMG CoA reduction to mevalonate, the thermodynamic properties of HMGCR binding with pravastatin were analyzed (38). HMG CoA reductase WT and mutant protein at a concentration of 20 µM in Buffer B supplemented with 1 mM NADPH in the reaction cell were injected with 50 µM pravastatin in Buffer B supplemented with 1 mM NADPH using the multiple injection mode for a total 20 7-µL injections. Heat data were plotted using Nano Analyze software™.

Anti-HMGCR Antibodies Assay. Serological examination of patient serum for anti-HMGCR autoantibodies was performed as described (39). Briefly, Nunc MaxiSorp™ plates were coated with 100 ng of WT HMGCR protein overnight at 4 °C. Diluted serum from patients and controls (1:200) was added to the plate and incubated 1 h at 37 °C. Plates were washed and incubated with a rabbit anti-human-HRP antibody (ab5679, Abcam). Plates were developed using the Pierce™ TMB Substrate Kit (Thermo) and analyzed with an Infinite M200 plate reader (Tecan). Rabbit anti-HMGCR antibody 1:5,000 and PBS were used as positive and negative controls, respectively.

Generation of CRISPR Cell Line. SH-SY5Y (ATCC, VA, USA) cells were grown in 12-well plates and transfected using the PEI method to induce CRISPR KI with 0.5µg pX459 plasmid, cloned with two sets of sgRNA sets targeting *HMGCR* gene (see plasmids and primers list), in proximity to the c.2306G>A; NM_000859.3 mutation site, along with 2 µL 10 µM solution of an ssODN repair template for KI induction through homology directed repair. Cells were selected with an escalating dose of puromycin 0.2 to 2 µg/mL over 1 wk until no live cells remained in a control well. The cells were diluted and seeded in 96-well plates to yield 0.5 cell per well. Cells were then grown to confluency, detached from the well surface using trypsin-EDTA, and DNA was extracted from half of the cell solution using QuickExtract™ (Lucigen), while the remaining half was reseeded. The colonies were screened for the presence of the *HMGCR* mutation using the same RFLP mentioned above.

Microscopy. SH-SY5Y cells harboring a CRISPR-KI-induced c.2306G>A mutation, as well as control cells, were grown on coverslips in 12-well plates. Twenty-four hours after plating, the cells were transfected with plasmids encoding fluorescent proteins that localize to the endoplasmic reticulum and the plasma membrane (40, 41) using PEI. Twenty-four hours later, cells were fixed with 4% PFA, permeabilized with Triton X-100 and blocked with 0.5% FBS. Cells were stained for HMGCR with rabbit anti-HMGCR antibody, following by anti-rabbit 488 (ab150077, Abcam). Coverslips were mounted on slides using mounting medium with DAPI (ab104139, Abcam) and sealed with nail varnish. Slides were scanned using a Zeiss LSM880 confocal laser scanning microscope, and images were processed using Fiji software. Experiments were repeated three times.

Bioreactor Synthesis of Mevalonolactone. A flow chart of the synthesis and purification of mevalonolactone can be seen in *SI Appendix*, Fig. S2*A*. Mevalonolactone synthesis was performed using bacterial fermentation in a bioreactor. DH10B-strain *Escherichia coli* cells, harboring the pMevT plasmid (42), were cultured overnight at 37 °C, 180 RPM in a 250-mL shaker flask containing 100 mL of LB media supplemented with 30 µg/mL chloramphenicol. The culture was then used to inoculate a 10-L benchtop Jupiter bioreactor (Solaris), containing 6 L TB (20 g/L tryptone, 24 g/L yeast extract, 4 mL/L glycerol) media supplemented with 30 µg/mL chloramphenicol, 0.01% antifoam, 0.5 M sorbitol, and 25 mM betaine. The bioreactor was maintained at 37 °C until the biomass reached OD_{600} =30 to 60, after which the culture was induced using 1 mM IPTG, and the temperature was reduced to 32 °C and maintained at that for the entire duration of fermentation. During fermentation, the pH was set at 7.0 ± 0.1 by automatic addition of 25% ammonium hydroxide, dissolved oxygen (DO) was maintained at 30% by a cascade function adjusting stirring rate, air flow, and lastly O_2 flow, and the culture was fed 40% glucose solution. The glucose concentration was kept under 0.5 g/L (50 mg/dL) using either manual tuning of glucose feeding speed or by pH-stat feeding by a logic loop maintaining that whenever pH raises above seven, glucose flow is initiated at a rate of 0.1 mL/min, and when pH drops below seven, glucose flow is stopped. Antifoam was added automatically. DO, pH, and temp were monitored off-site using the Solaris software and were also monitored and adjusted every 4 h, when manually measuring OD_{600} and glucose levels. Fermentation batches were cultured for 16 to 120h. Additional

chloramphenicol and IPTG were added every 12 h. Example of a fermentation batch process can be seen in *SI Appendix*, Fig. S2*B*.

Extraction and Purification of Mevalonolactone. Cell culture broth was centrifuged at 12,000 g, 4 °C for 10 min, cell pellets were discarded, and the remaining broth was acidified to pH = 2 using 16% HCl and incubated at 45 °C to facilitate the conversion of mevalonic acid to mevalonolactone and the later organic extraction stage. The solution was saturated with NaCl and the resulting protein precipitates were discarded after either filtration using standard filter paper, centrifugation at 12,000 g, 4 °C, for 10 min, or both. The broth was then cooled and extracted for a minimum of three times using ethyl acetate in a 1 L separatory funnel. Hard emulsions were either discarded or centrifuged at 3,000 g for 5 min in glass tubes, and phases were separated and collected. The organic phase was evaporated using a rotary evaporator, and the remaining mevalonolactone was placed under high vacuum (10^{-3} torr) overnight.

Batches failing to show >94% purity by GC–MS were further purified by silica column chromatography, using ethyl acetate alone as the mobile phase. The GC–MS analysis was used to inspect the resulting fractions. Other samples were further purified using acid–base extraction—samples were dissolved in ultrapure water; pH was adjusted to 10, and the solution was extracted three times using ethyl acetate to remove all nonacidic components. The resulting solution was adjusted to pH of two and extracted three times with ethyl acetate. The organic phase was then dried as described.

Mevalonolactone Purity Analysis. Purity was inspected by GC–MS (43) and NMR. Samples were dissolved in ethyl acetate and subjected to GC–MS on an Agilent 5977A GC/MSD system–7890B Agilent GC system with an ultrainert GC column (19091S-433UI) followed by an Agilent 5977A MS instrument. Helium was used as the carrier gas at a constant flow of 0.7 mL/min, and 1:50 split samples were injected. Injection port and MS source temperature were held constant at 230 °C, and the MS quad temperature was held constant at 150 °C. The column temperature gradient was as follows: 70 °C for 0.5 min, 25 °C/min to 150 °C, 15 °C/min to 200 °C, and 25 °C/min to 300 °C and held at the upper temperature for 1 min. Results were analyzed on Mass Hunter software, the mass spectrum was compared to Wiley/NIST 2014 library (*SI Appendix*, Fig. S3*A*–*C*). For NMR analysis, samples were dissolved in deuterated chloroform ($CDCl_3$) in NMR tubes and were analyzed using an AVANCE III-400 device (Bruker) in ^{1}H, ^{13}C, and DEPT NMR modes. Resulting spectra were compared to National Institute of Advanced Industrial Science and Technology (AIST) spectral database. (*SI Appendix*, Fig. S3 *D* and *E*)

Mevalonolactone Toxicity Study in Mice. The safety of oral treatment with mevalonolactone was assessed by oral gavage. Gavage was performed using a 22-gauge olive tip curved gavage needle coated with a sugar solution (44), with 3 doses of 20, 200, and 2,000 mg/kg of mevalonolactone or 0.9% saline solution daily for 7 d to assess toxicity and chemical damage potential (n = 5 for each group). Blood samples were collected at day 0 from the mandibular vein. At day 7 mice were sacrificed, blood samples were collected, and organs were fixed with formalin, embedded in paraffin, sectioned, and stained with H&E and PAS. Slides were reviewed by an expert veterinary pathologist (Patho-Logica LTD).

Mevalonolactone LC–MS Analysis. Serum samples from patients and healthy volunteers were assessed by LC–MS. Sample preparation and chromatographic analysis were based on a previously described method (45). Briefly, 100 µL serum samples or mevalonolactone standard (25 to 0 ng/mL in an eight-point serial dilution with HPLC-grade water) was added to 200 µL of 0.1M HCl and was shaken for 30 min at room temperature. Organic extraction was performed by addition of 1 mL ethyl acetate. The samples were shaken at room temperature for 1 h, centrifuged at 3,000 g for 10 min, and 800 µL was transferred to a new HPLC vial and evaporated to dryness using a Savant SpeedVac™ (Thermo). Lastly, the samples were reconstituted in 100 µL of 80% methanol, 20% water, and 0.1% formic acid. Sample injections (10 µL) were separated on an Acquity HSS-T3 1.8 µm, 2.1 × 100 mm column and were analyzed in a Q Exactive focus hybrid quadrupole LC–MS system. The spectra were analyzed using FreeStyle™ software.

Mevalonolactone Treatment. The treatment trial was monitored by a senior neurologist, and safety and efficacy reports were issued to the Israeli MOH in accordance with standard procedure. The patient was instructed to contact a member of the trial staff in case of adverse events and to keep record of all adverse events or lack of them in writing.

The treatment protocol was planned as an escalating dose of oral mevalonolactone, a viscous liquid, dissolved in water or encapsulated in gelatin caps, given once weekly. The treatment plan can be seen in supplemental *SI Appendix*, Fig. S4*A*. The treatment plan was modified to facilitate the patients' needs, coincidental events, and therapeutic goals, as seen in *SI Appendix*, Fig. S4*B*. During treatment, the patient was monitored closely, with weekly questioning, physical examination, spirometry, blood tests, and manual muscle dynamometry using a hand-held dynamometer (HHD; Lafayette instruments®) done by a member of the trial staff and bimonthly exam by a senior neurologist including MMT. Due to the condition of the patient, including inability to ambulate because of severe muscle weakness and ventilator dependence, HHD was favored over tests such as 6-min walk test, as was done previously in patients with LGMD (46) HHD was not initiated until 28 d into the study according to patient request and was initially replaced with hand-grip dynamometry which, later deemed ineffective for this purpose. Whole-body MRI, thorough blood investigation, echocardiography, abdominal ultrasound, EMG, and NCV tests were done prior to commencement of treatment and 1 y into the treatment.

Mevalonolactone Treatment in Mice. C57BL/6. mice (purchased from Harlen) were randomized to six treatment groups.

1. Cerivastatin (ab142853, abcam) 1 mg/kg/d IP with/without 200 mg/kg/d mevalonolactone in drinking water. Cerivastatin was injected at a concentration of 0.3 mg/mL; the injection volume was calculated by animal weight. n = 4 each
2. Simvastatin, alkaline hydrolyzed (47) (sc-200829, Santa Cruz biotechnology) 20 mg/kg/d IP with/without 200 mg/kg/d mevalonolactone in drinking water. Simvastatin was injected at a concentration of 5.4 mg/mL; the injection volume was calculated by animal weight. n = 4 each
3. Sterile 0.9% saline solution IP with/without 200 mg/kg/d mevalonolactone in drinking water. n = 4 each

For mevalonolactone treatment at an estimated dosage of 200 mg/kg/d, mice were given free access to drinking water containing 1.55 g/L mevalonolactone, based on average mouse weight of 25 to 30 g and average daily water intake of 3.5 mL. The treatment was initiated at age 8 wk for a duration of 14 d. Mice were injected and monitored daily and weighed every 3 d. Assessment of muscle strength and endurance was performed using the hanging wire assay at day 0 and at days 4, 7, 11, and 14, a strength test using a grip strength meter 1027SM (Columbus Instruments) on day 14 and by measuring locomotor activity in a PhenoMaster home-cage phenotyping system (TSE systems) equipped with ActiMot3 and Voluntary Running Wheel modules from days 11 to 14. At the end of day 14, mice were killed by inhalation of isoflurane followed by cervical dislocation, and blood and organs were collected.

Statistical Analysis. All results were analyzed using GraphPad Prism V9 (La Jolla, CA, USA) with student t test, ANOVA analysis, and Michaelis–Menten kinetics studies. Data from multiple PhenoMaster experiments of a particular intervention was normalized to a single experiment and outlier, and outliers were excluded. Data from PhenoMaster was also evaluated using CalR software (48). Significance was set at a confidence level of 0.05, In all figures, ns denotes $P \geq 0.05$, * denotes $P < 0.05$, ** $P < 0.01$, denotes *** $P < 0.001$, and **** denotes $P < 0.0001$. Data represent mean ± SD.

Study Approval. All human studies and were performed following SUMC IRB approval and written informed consent. Treatment of patients with mevalonolactone was conducted under the approval and supervision of the SUMC drug committee and the Israeli MOH under an "expanded access / compassionate use" protocol, given the severe condition of patients and the lack of alternative treatments for LGMD associated with *HMGCR* mutation. The patient treated was instructed as to the risks and possible benefits and granted signed informed consent.

All animal studies were conducted under the approval of IACUC committee and in accordance with standards of animal care.

Data, Materials, and Software Availability. All study data, apart from detailed whole-exome sequencing data, are included in the article and/or supplementary

files. Whole-exome sequencing data used in the current study are available in the Sequence Read Archive (SRA) repository https://www.ncbi.nlm.nih.gov/bioproject/PRJNA925668.

ACKNOWLEDGMENTS. The research was funded by the Israel Science Foundation (grant no. 2034/18) awarded to O.S.B., as well as by a scholarship to Y.Y. from the Foulkes foundation, and by the National Knowledge Center for Rare/Orphan Diseases of the Israel Ministry of Science, Technology and Space, Ben-Gurion University of the Negev, Beer-Sheva, Israel. We are thankful for the advice and support throughout the project from the labs of Michael Meijler, Niv Papo, and Amir Tirosh, as well as Daniel Flusser, Anna Nikonov, Ron Dabby, Shimon Ben-Shabat, Noash el-Atzibi, David Stepensky, Uzi Hadad, Anat Shahar, Inbal Berkowitz, Zehavit Dadon, Shmuel Springer, and Victor Novack. We thank the patients and their families for their efforts and collaboration in the study.

Author affiliations: [a]The Morris Kahn Laboratory of Human Genetics at the National Institute of Biotechnology in the Negev, Ben-Gurion University of the Negev, Beer Sheva, 8410501 Israel; [b]Department of Pediatric Neurology, Soroka University Medical Center, Faculty of Health Sciences, Ben-Gurion University of the Negev, Beer Sheva, 8410101 Israel; [c]Genetics Institute, Soroka University Medical Center, Faculty of Health Sciences, Ben-Gurion University of the Negev, Beer Sheva, 8410101 Israel; [d]Department of Life Sciences, Ben-Gurion University of the Negev, Beer Sheva, 8410501 Israel; [e]National Institute for Biotechnology in the Negev and Ilse Katz Institute for Nanoscale Science and Technology, Ben-Gurion University of the Negev, Beer Sheva, 8410501 Israel; and [f]Department of Radiology, Soroka University Medical Center and the Faculty of Health Sciences, Ben-Gurion University of the Negev, Beer-Sheva, 8410101 Israel

1. E. Mercuri, C. G. Bönnemann, F. Muntoni, Muscular dystrophies. *Lancet* **394**, 2025–2038 (2019).
2. A. P. Murphy, V. Straub, The classification, natural history and treatment of the limb girdle muscular dystrophies. *J. Neuromuscul. Dis.* **2**, S7–S19 (2015).
3. E. Pozsgai *et al.*, Unmet needs and evolving treatment for limb girdle muscular dystrophies. *Neurodegener. Dis. Manag.* **11**, 411–429 (2021).
4. F. Taylor, Statins for the primary prevention of cardiovascular disease. *Cochrane Database Syst. Rev.* **2017**, CD004816 (2013).
5. C. Baigent *et al.*, Efficacy and safety of cholesterol-lowering treatment: Prospective meta-analysis of data from 90,056 participants in 14 randomised trials of statins. *Lancet* **366**, 1267–78 (2005).
6. J. T. Davies *et al.*, Current and emerging uses of statins in clinical therapeutics: A review. *Lipid Insights* **9**, 13–29 (2016).
7. P. Mohassel, A. L. Mammen, Anti-HMGCR myopathy. *J. Neuromuscul. Dis.* **5**, 11–20 (2018).
8. N. C. Ward, G. F. Watts, R. H. Eckel, Statin toxicity: Mechanistic insights and clinical implications. *Circ. Res.* **124**, 328–350 (2019).
9. R. Bitzur, H. Cohen, Y. Kamari, D. Harats, Intolerance to statins: Mechanisms and management. *Diabetes Care* **36**, S325–30 (2013).
10. B. A. Golomb, M. A. Evans, Statin adverse effects: A review of the literature and evidence for a mitochondrial mechanism. *Am. J. Cardiovasc. Drugs* **8**, 373–418 (2008).
11. E. Mercuri, F. Muntoni, Muscular dystrophies. *Lancet* **381**, 845–860 (2013).
12. D. Fischer, M. P. Wattjes, *MRI in Muscle Dystrophies and Primary Myopathies* (Springer, Berlin, Heidelberg, 2013), pp. 241–254.
13. S. A. Peters *et al.*, MRI in lipid-lowering agent-associated myopathy: A retrospective review of 21 cases. *Am. J. Roentgenol.* **194**, W323–W328 (2010).
14. I. Pinal-Fernandez *et al.*, Thigh muscle MRI in immune-mediated necrotising myopathy: Extensive oedema, early muscle damage and role of anti-SRP autoantibodies as a marker of severity. *Ann. Rheum. Dis.* **76**, 681–687 (2017).
15. R. M. Turner, M. Pirmohamed, Statin-related myotoxicity: A comprehensive review of pharmacokinetic, pharmacogenomic and muscle components. *J. Clin. Med.* **9**, 22 (2020).
16. Y. Zhu *et al.*, Serum enzyme profiles differentiate five types of muscular dystrophy. *Dis. Markers* **2015**, 543282 (2015).
17. E. S. Istvan, J. Deisenhofer, Structural mechanism for statin inhibition of HMG-CoA reductase. *Science* **292**, 1160–1164 (2001).
18. S. Richards *et al.*, Standards and guidelines for the interpretation of sequence variants: A joint consensus recommendation of the american college of medical genetics and genomics and the association for molecular pathology. *Genet. Med.* **17**, 405–424 (2015).
19. Y. Osaki *et al.*, Skeletal muscle-specific HMG-CoA reductase knockout mice exhibit rhabdomyolysis: A model for statin-induced myopathy. *Biochem. Biophys. Res. Commun.* **466**, 536–540 (2015).
20. J. J. Shen *et al.*, The role of clinical response to treatment in determining pathogenicity of genomic variants. *Genet. Med.* **23**, 581–585 (2021).
21. H. R. Chung *et al.*, The impact of exercise on statin-associated skeletal muscle myopathy. *PLoS One* **11**, e0168065 (2016).
22. B. M. Meador, K. A. Huey, Statin-associated changes in skeletal muscle function and stress response after novel or accustomed exercise. *Muscle Nerve* **44**, 882–889 (2011).
23. K. E. Hansen, J. P. Hildebrand, E. E. Ferguson, J. H. Stein, Outcomes in 45 patients with statin-associated myopathy. *Arch. Intern. Med.* **165**, 2671–2676 (2005).
24. M. Abdulrazaq, F. Hamdan, W. Al-Tameemi, Electrophysiologic and clinico-pathologic characteristics of statin-induced muscle injury. *Iran. J. Basic Med. Sci.* **18**, 737–744 (2015).
25. A. Selva-O'Callaghan *et al.*, Statin-induced myalgia and myositis: An update on pathogenesis and clinical recommendations. *Expert Rev. Clin. Immunol.* **14**, 215–224 (2018).
26. R. S. Rosenson, S. K. Baker, T. A. Jacobson, S. L. Kopecky, B. A. Parker, An assessment by the statin muscle safety task force: 2014 update. *J. Clin. Lipidol.* **8**, S58–S71 (2014).
27. K. Ohashi *et al.*, Early embryonic lethality caused by targeted disruption of the 3-hydroxy-3-methylglutaryl-CoA reductase gene. *J. Biol. Chem.* **278**, 42936–42941 (2003).
28. A. Alshehri, R. Choksi, R. Bucelli, A. Pestronk, Myopathy with anti-HMGCR antibodies Perimysium and myofiber pathology. *Neurol. Neuroimmunol. NeuroInflamm.* **2**, e124 (2015).
29. T. R. Joy, Narrative review: Statin-related myopathy. *Ann. Intern. Med.* **150**, 858 (2009).
30. C. M. Schooling, S. L. Au Yeung, G. Freeman, B. J. Cowling, The effect of statins on testosterone in men and women, a systematic review and meta-analysis of randomized controlled trials. *BMC Med.* **11**, 57 (2013).
31. J. P. Crandall *et al.*, Statin use and risk of developing diabetes: Results from the diabetes prevention program. *BMJ Open Diabetes Res. Care* **5**, e000438 (2017).
32. F. A. Wood *et al.*, N-of-1 trial of a statin, placebo, or no treatment to assess side effects. *N. Engl. J. Med.* **383**, 2182–2184 (2020).
33. V. Straub *et al.*, 229th ENMC international workshop: Limb girdle muscular dystrophies - Nomenclature and reformed classification Naarden, the Netherlands, 17–19 March 2017. *Neuromuscul. Disord.* **28**, 702–710 (2018).
34. O. Wormser *et al.*, SCAPER localizes to primary cilia and its mutation affects cilia length, causing Bardet-Biedl syndrome. *Eur. J. Hum. Genet.* **27**, 928–940 (2019).
35. D. Seelow, M. Schuelke, F. Hildebrandt, P. Nürnberg, HomozygosityMapper - An interactive approach to homozygosity mapping. *Nucleic Acids Res.* **37** (2009).
36. M. Silberstein *et al.*, A system for exact and approximate genetic linkage analysis of SNP data in large pedigrees. *Bioinformatics* **29**, 197–205 (2013).
37. E. S. Istvan, M. Palnitkar, S. K. Buchanan, J. Deisenhofer, Crystal structure of the catalytic portion of human HMG-CoA reductase: Insights into regulation of activity and catalysis. *EMBO J.* **19**, 819–830 (2000).
38. T. Carbonell, E. Freire, Binding thermodynamics of statins to HMG-CoA reductase. *Biochemistry* **44**, 11741–11748 (2005).
39. A. L. Mammen *et al.*, Autoantibodies against 3-hydroxy-3-methylglutaryl-coenzyme a reductase in patients with statin-associated autoimmune myopathy. *Arthritis Rheum.* **63**, 713–721 (2011).
40. J. Goedhart *et al.*, Structure-guided evolution of cyan fluorescent proteins towards a quantum yield of 93%. *Nat. Commun.* **3**, 751 (2012).
41. R. L. Strack *et al.*, A rapidly maturing far-red derivative of DsRed-Express2 for whole-cell labeling. *Biochemistry* **48**, 8279–8281 (2009).
42. V. J. J. Martin, D. J. Piteral, S. T. Withers, J. D. Newman, J. D. Keasling, Engineering a mevalonate pathway in Escherichia coli for production of terpenoids. *Nat. Biotechnol.* **21**, 796–802 (2003).
43. S. M. Ma *et al.*, Optimization of a heterologous mevalonate pathway through the use of variant HMG-CoA reductases. *Metab. Eng.* **13**, 588–597 (2011).
44. A. F. Hoggatt, J. Hoggatt, M. Honerlaw, L. M. Pelus, A spoonful of sugar helps the medicine go down: A novel technique to improve oral gavage in mice. *J. Am. Assoc. Lab. Anim. Sci.* **49**, 329–334 (2010).
45. R. N. Cestari *et al.*, Plasma mevalonic acid exposure as a pharmacodynamic biomarker of fluvastatin/atorvastatin in healthy volunteers. *J. Pharm. Biomed. Anal.* **182**, 1–7 (2020).
46. M. C. Walter *et al.*, Treatment of dysferlinopathy with deflazacort: A double-blind, placebo-controlled clinical trial. *Orphanet J. Rare Dis.* **8**, 26 (2013).
47. B. P. Leung *et al.*, A novel anti-inflammatory role for simvastatin in inflammatory arthritis. *J. Immunol.* **170**, 1524–1530 (2003).
48. A. I. Mina *et al.*, CalR: A web-based analysis tool for indirect calorimetry experiments. *Cell Metab.* **28**, 656–666.e1 (2018).